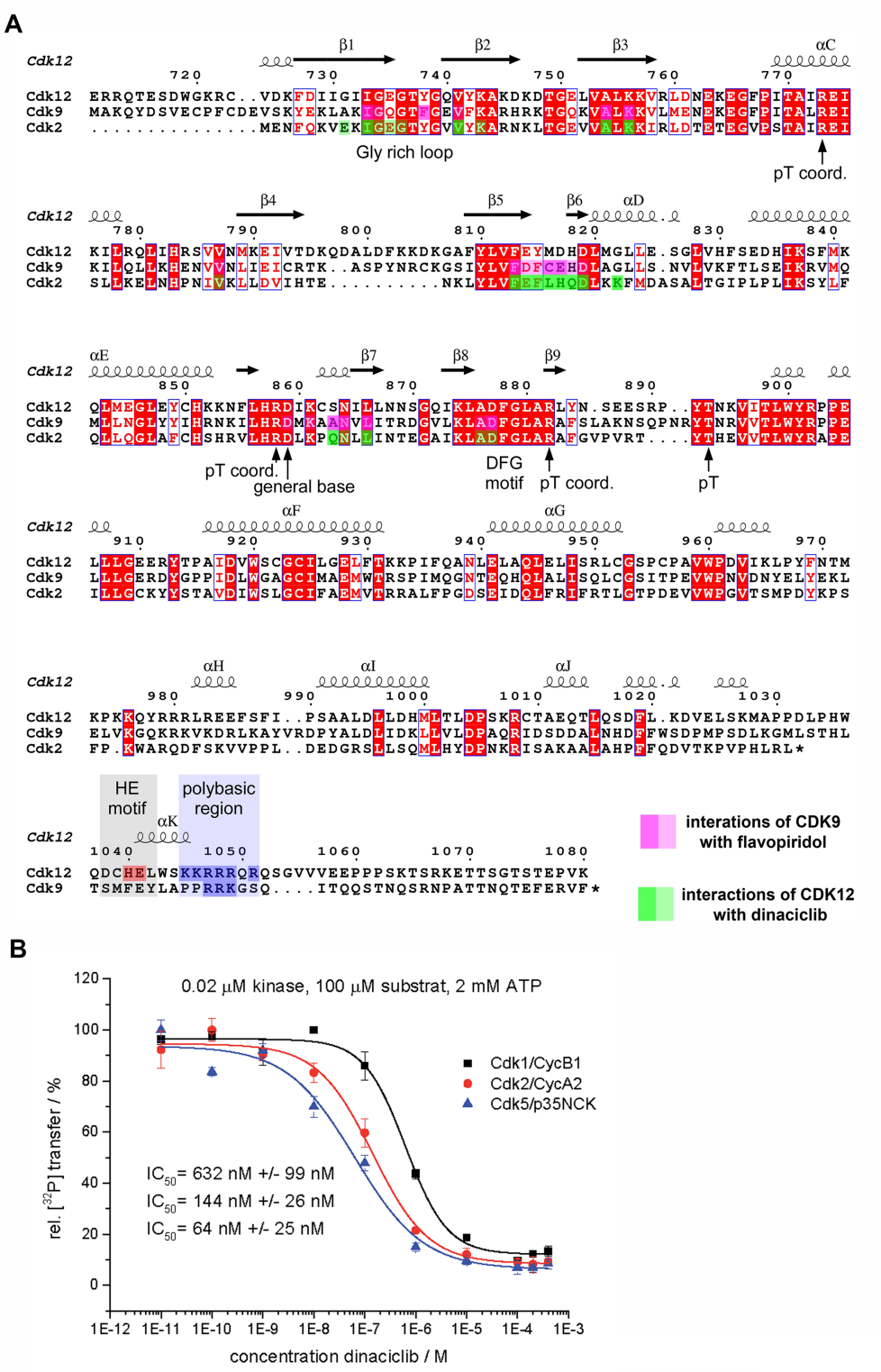

Figure S1. Related to Figure 1.

(A) Sequence alignment of human kinases CDK2, CDK9, and CDK12. The transcription-regulating kinases CDK9 and CDK12 contain a C-terminal extension helix that is composed of an HE-motif and a conserved polybasic region. The extension helix interacts with the ATP moiety of the kinase active site, which is enabled by a glycine residue (G822) in helix αD. In contrast, the cell cycle-regulating kinase CDK2 does not contain such extension helix but harbors a lysine at the site of the glycine in CDK9 and CDK12. Residues in CDK2 that directly interact with dinaciclib are colored green (PDB accession code 4KD1; Martin et al., 2013). Residues in CDK2 whose accessibility is impaired by dinaciclib are colored light green. Residues of CDK9 interacting with flavopiridol are colored rose (3BLR; Baumli et al., 2008). Secondary structure elements are indicated for CDK2 above the sequence. Residues conserved in all CDKs are boxed red and those that are similar are colored red. The UniProt accession numbers are Q9NYV4 (CDK12, human), P50750 (CDK9, human), and P24941 (CDK2, human). The sequence alignment was prepared with MultAlin, and the secondary structure alignment was prepared with ESPript.

(B) Concentration series for dinaciclib against CDK1, CDK2 and CDK5 holoenzymes. IC_{50} values using 0.02 μM kinase are indicated.

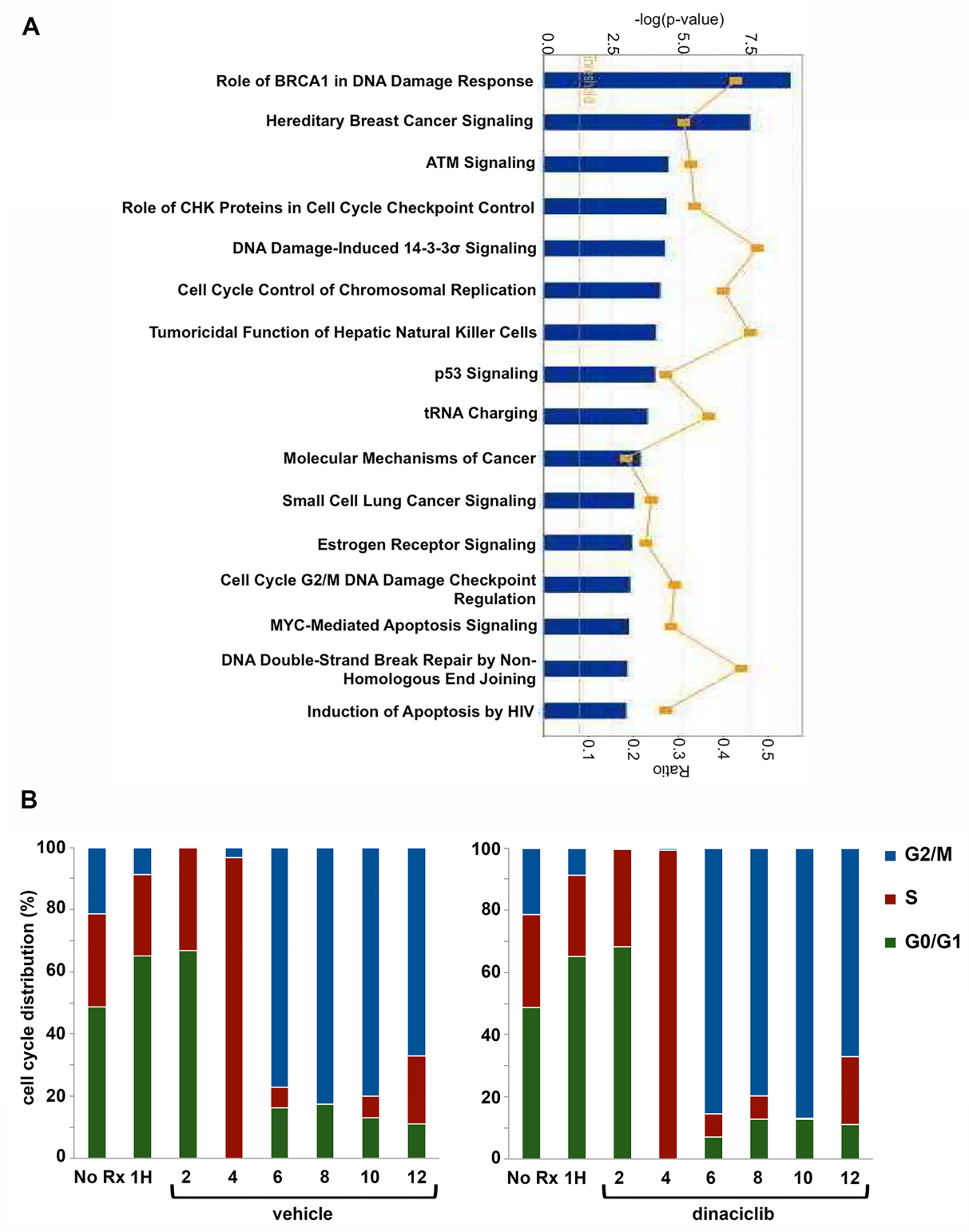

Figure S2. Related to Figure 2.

(A) Ingenuity Pathway Analysis of genes statistically significantly downregulated in response to dinaciclib. Genes involved in the DNA damage response and in DNA repair pathways are among the most prominently down-regulated.

(B) S Phase progression in dinacicib-treated cells. MDA-MB-231 cells were treated with 1 mM hydroxyurea for 24 hours, in order to achieve synchronization at the G1/S boundary (1H). Cells were then released into vehicle or 10 nM dinaciclib. Progression through S phase over the next 12 hours was monitored by flow cytometry, demonstrating similar rates of S phase progression in vehicle and dinaciclib-treated cells.

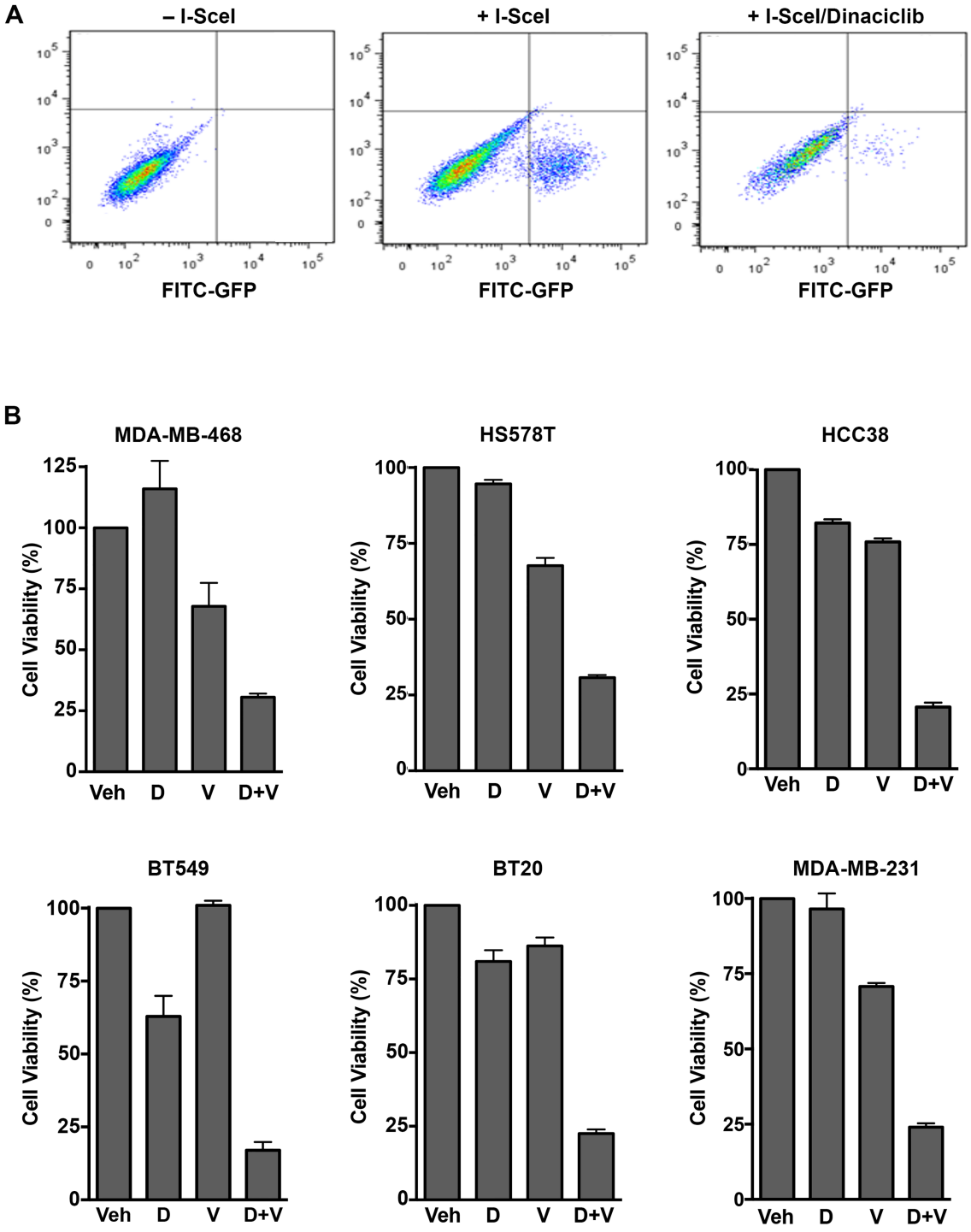

Figure S3. Related to Figure 3.

(A) Dinaciclib directly inhibits HR. U2OS pDR-GFP cells transfected with an I-SceI cutting enzyme in the presence of vehicle or 15 nM dinaciclib, analyzed for GFP expression by flow cytometry. The data demonstrate the decrease in the percentage of GFP-positive cells in the presence of dinaciclib, consistent with direct inhibition of HR repair, and are quantified in Figure 3C.

(B) Cell viability of BRCA-proficient TNBC cell lines were treated with vehicle, dinaciclib, veliparib or the combination. Bar graphs are related to the data shown in Figure 3D. Cell viability is shown following exposure to vehicle, 200 μM veliparib, 5-10 nM dinaciclib or the combination.

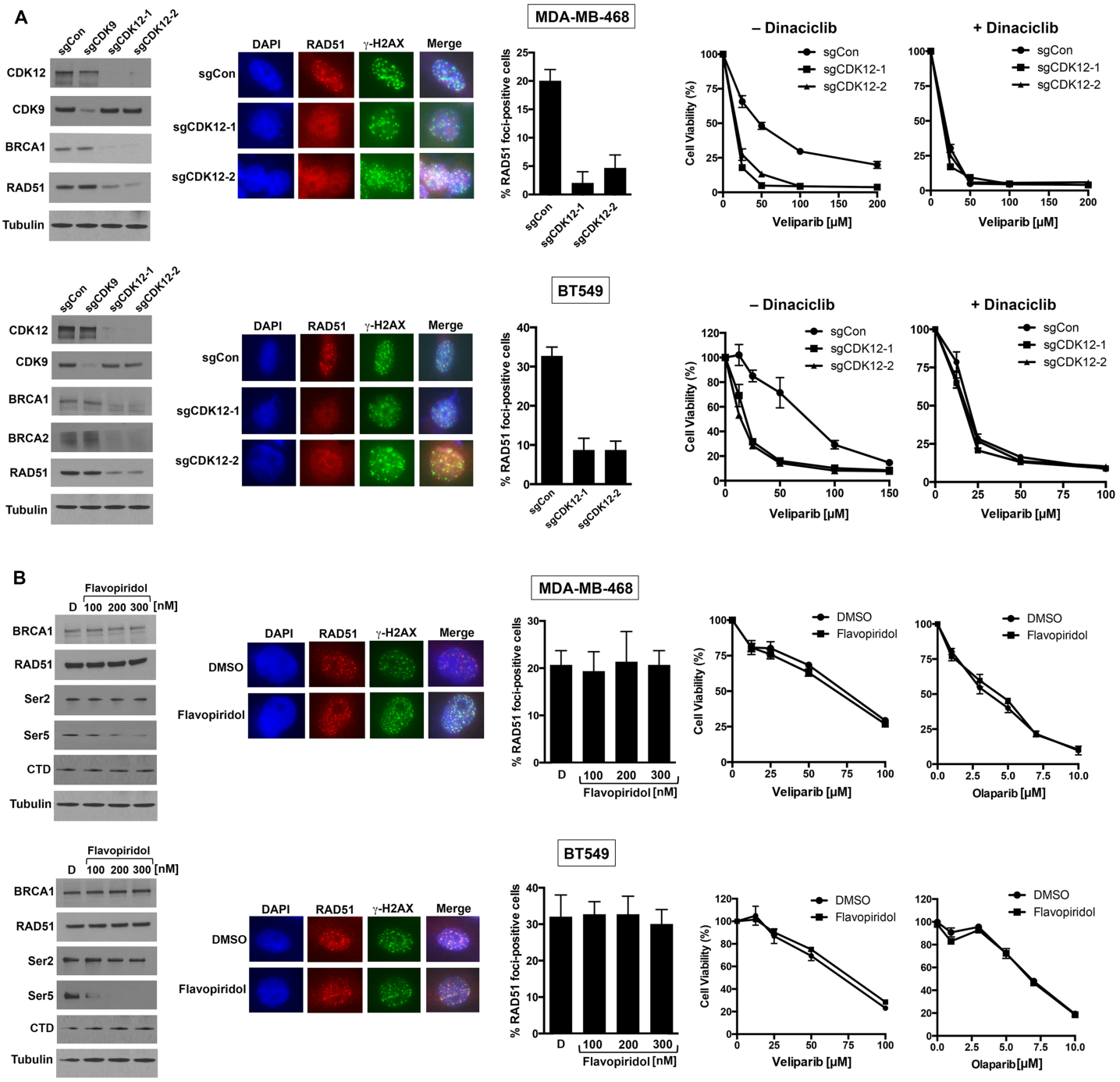

Figure S4. Related to Figure 3.

(A) CDK12 knockout phenocopies the effects of dinaciclib in MDA-MB-468 and BT5479 TNBC cells. CRISPR/Cas9-mediated knockdown of CDK12 (but not CDK9) causes reduced expression of BRCA proteins and RAD51, as well as reduced RAD51 foci 6 hours after 10 Gy γ-irradiation. Representative cells subjected to immunofluorescence for RAD51 and γ-H2AX are shown, with quantification of the percentage of cells with ≥ five RAD51 foci. CDK12 knockdown sensitizes cells to veliparib; the addition of 10 nM dinaciclib sensitizes control cells to veliparib but does not further sensitize cells in which CDK12 is already depleted.

(B) Flavopiridol-mediated CDK9 inhibition does not sensitize cells to PARP inhibition. Flavopiridol reduced phosphorylation of the RNA polymerase II C-terminal domain (CTD) at Ser5 and not Ser2, consistent with CDK9 inhibition. In the presence of flavopiridol, formation of RAD51 foci after γ-irradiation is intact, and TNBC cells are not sensitized to either veliparib or olaparib.

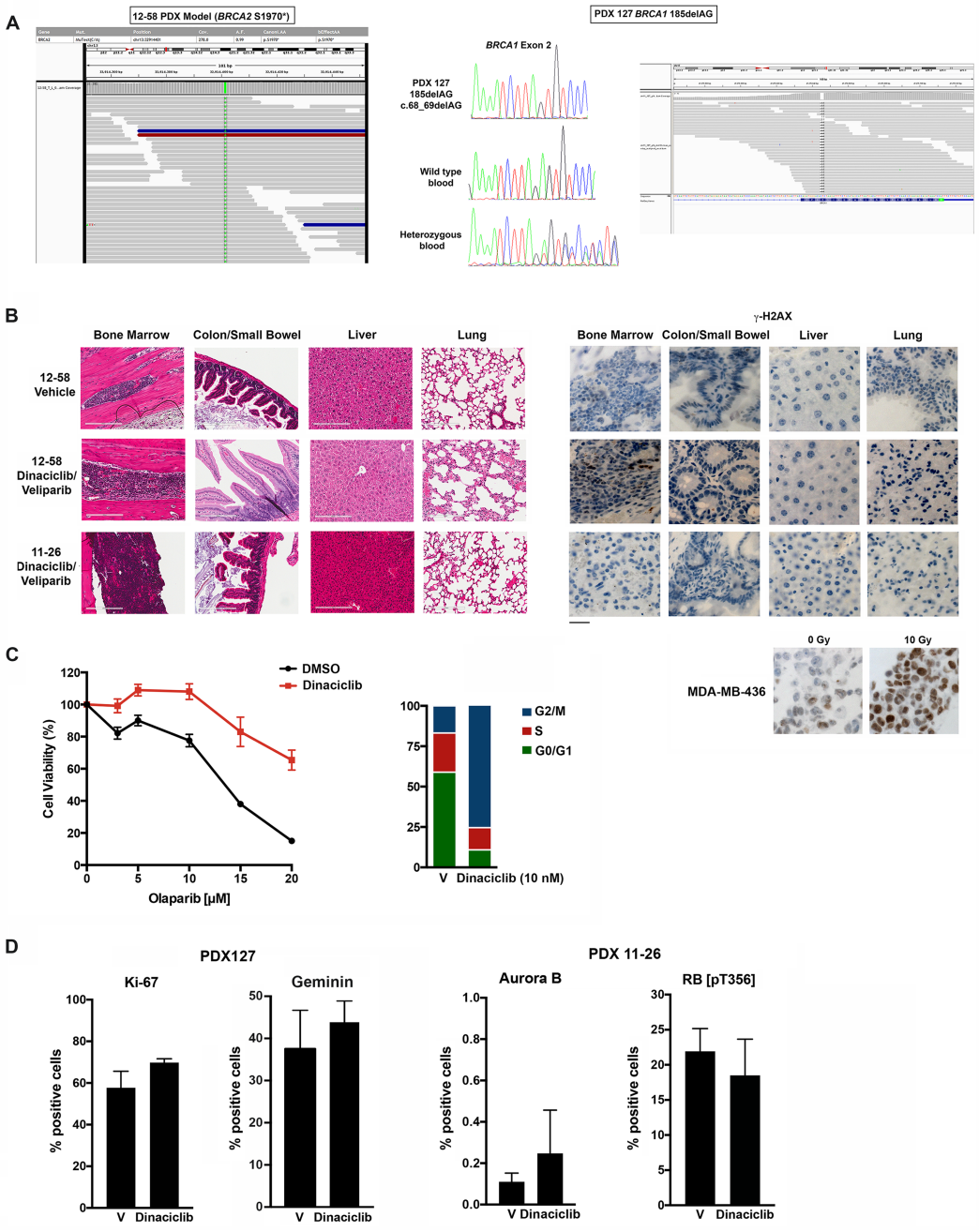

Figure S5. Related to Figures 3, 6 and 7.

(A) Sequencing of PARP inhibitor-resistant PDX models reveals absence of *BRCA* reversion mutations. *(Left)* Visualization of sequencing reads confirming *BRCA2* 1970* mutation in the 12-58 PDX model. *(Middle)* Sanger view demonstrating *BRCA1* del185AG mutation with loss of heterozygosity in the PDX127 xenograft derived from the patient's tumor. *(Right)* IGV view of sequencing reads confirming *BRCA1* 185delAG in the PDX127 model.

(B) Lack of end-organ toxicity in mice treated with the dinaciclib/veliparib combination. *(Left)* Histology from bone marrow, colon or small bowel, liver and lung harvested from mice treated with vehicle or the dinaciclib/veliparib combination at the end of the experiments shown in Figures 3G and 7A for the 12-58 and 11-26 PDX models, respectively. For the 11-26 model, mice were euthanized at day 154, demonstrating that long-term treatment with the dinaciclib/veliparib combination does not induce end-organ toxicity. *Bars,* 200 μm. *(Right)* Bone marrow, GI tract, liver and lung tissues were stained for γ-H2AX. Representative sections are shown. In the 12-58 model, ~5% of cells in the bone marrow stained positively for γ-H2AX, while other organs were negative from each of four mice analyzed that were treated with the dinaciclib/veliparib combination, similar to the findings in vehicle-treated mice. In the 11-26 model only rare cells were positive for γ-H2AX staining in 5 of 6 mice analyzed that were treated with the combination; in the sixth mouse there was modest staining in the bone marrow and focal γ-H2AX-positivity in colonic crypts and bronchial epithelium. *Bar*, 100 μm.

(C) Human mammary epithelial cells (HMECs) are insensitive to combined dinaciclib and PARP inhibition. *(Left)* HMECs were treated with olaparib in the absence or presence of dinaciclib; viability was improved in the presence of dinaciclib. *(Right)* Dinaciclib induces G2/M arrest in HMECs.

(D) Dinaciclib-treated patient-derived xenografts are proliferating at a time when BRCA1 and RAD51 mRNA and protein expression are reduced. Tumor sampling occurred at early time points (15 days for PDX127 and 22-37 days for PDX 11-26). For PDX127, tumors from vehicle and dinaciclib-treated mice were stained with Ki-67 or geminin (vehicle: n = 5 for Ki-67 and n = 2 for geminin; dinaciclib: n = 6 for Ki-67 and n = 2 for geminin). For PDX-11-26, vehicle (n = 2) and dinaciclib (n = 4) –treated mice were stained for Aurora B and phosphorylated RB [pT356], a site modulated by dinaciclib (Mita et al., 2011). At these time points, there were no statistically significant changes in Ki-67, geminin, Aurora B and phospho-RB staining between vehicle and dinaciclib-treated tumors, indicating that cell cycle arrest does not account for reduced HR gene and protein expression in these models.

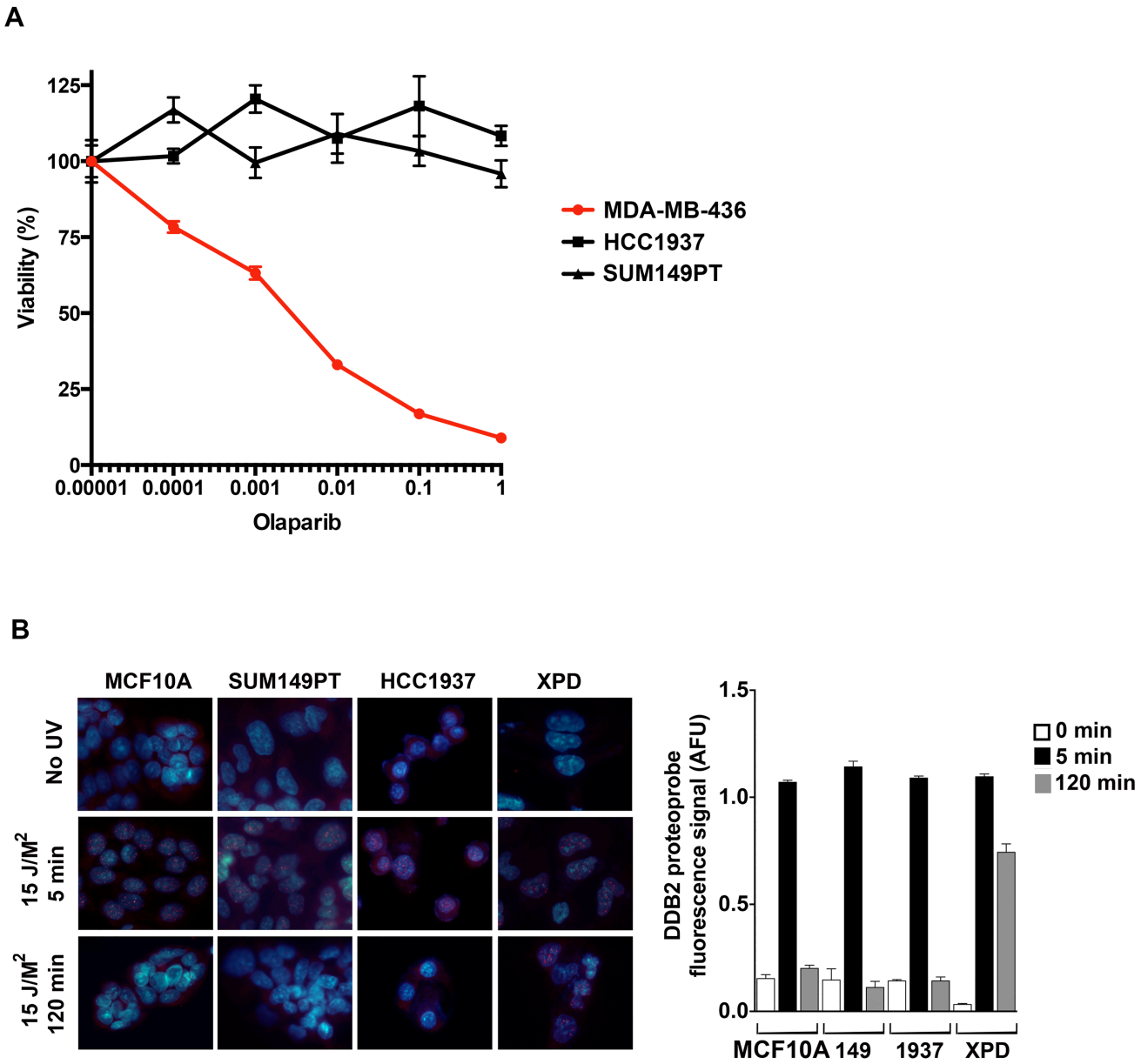

Figure S6. Related to Figure 4.

(A) *BRCA1*-mutated HCC1937 and SUM149 cells are resistant to olaparib. MDA-MB-436, HCC1937 and SUM149PT cells were treated with the indicated concentrations of olaparib and viability assessed after 7 days of treatment. These data demonstrate that despite *BRCA1* mutation, HCC1937 and SUM149PT are resistant to olaparib, as well as veliparib.

(B) The platinum sensitivity of these cell lines is not explained by defects in nucleotide excision repair (NER). The indicated cell lines were fixed intact or 5 and 120 minutes after irradiation with 15J/m^2 UV-C and analyzed for (6-4) photoproducts using the DDB2 proteo-probe (red). DNA was visualized using DAPI (blue). NER status was calculated from the image quantification.

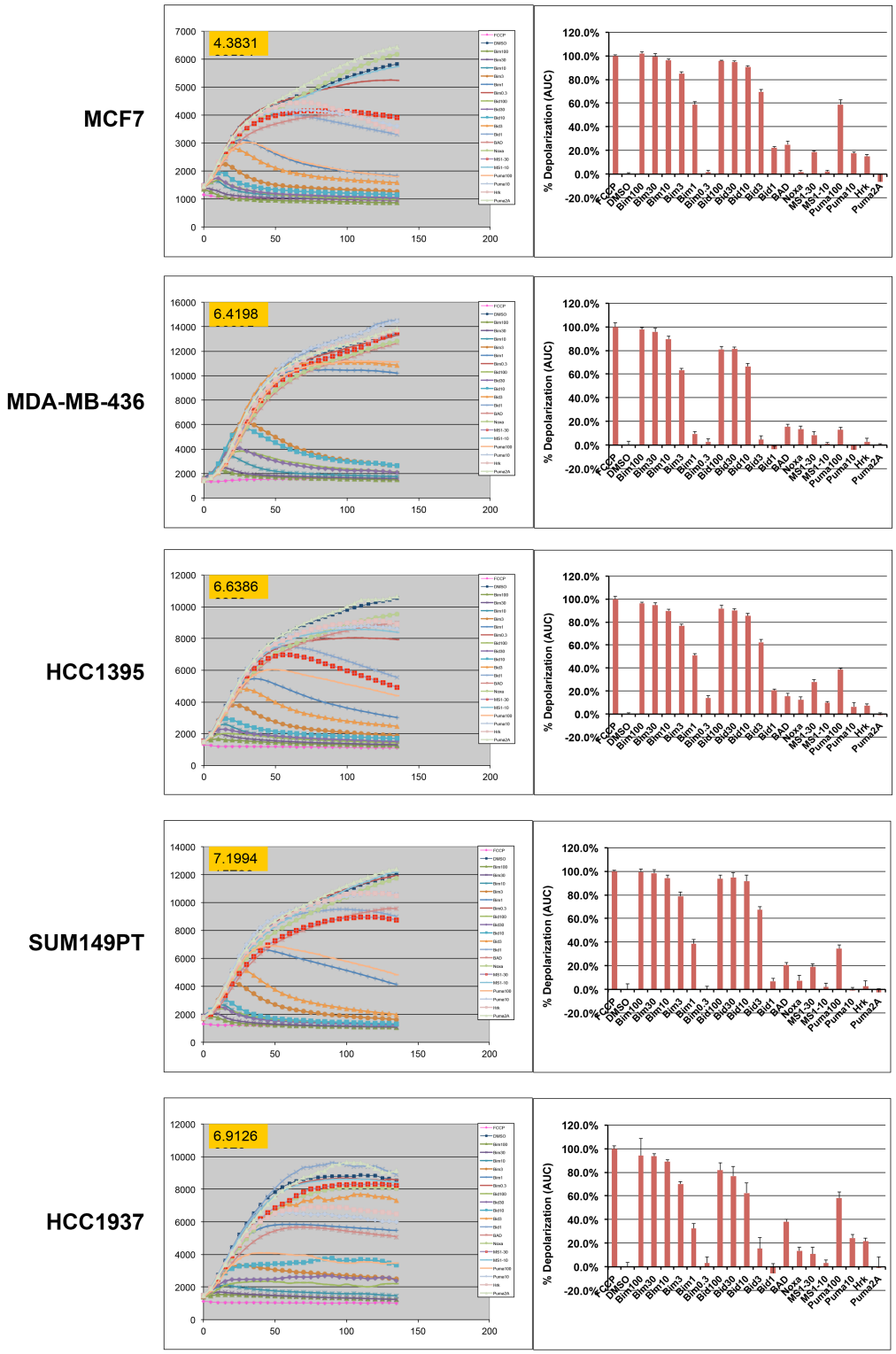

Figure S7. Related to Figure 4.

BH3 profiling of TNBC cell lines. Proliferating cells that were 30-50% confluent were harvested and counted for BH3 profiling. The number at the top left of each graph represents the ratio of signal from DMSO treated cells to those treated with the positive control FCCP (p-trifluoromethoxy carbonyl cyanide phenyl hydrazone). A number above 3 indicates that a sufficient number of mitochondria were analyzed (sufficient signal to noise ratio for analysis). The data demonstrate that all of the cell lines are relatively primed with robust responses to the BIM and BID peptides, indicating that cells contain functional BAX/BAK and do not have an abundance of unbound anti-apoptotic proteins. Additionally, high responses are not observed to the BAD (inhibits BCL2 and BCL-xL) nor MS1 (inhibits MCL1) peptides, indicating that cells are not very dependent on BCL2, BCL-xL or MCL1 for survival, i.e. these proteins are not actively sequestering high amounts of pro-apoptotic BIM and BID.

Table S1: Dinaciclib-Mediated Sensitization of TNBC Cell Lines to Veliparib

(Related to Figures 3 and 5)

Cell Line	IC_{50} veliparib (μM) (– dinaciclib)	IC_{50} veliparib (μM) (+ dinaciclib)
***BRCA1* Wild Type/HR-Proficient**		
MDA-MB-468	71.5	5.7
HS578T	102.2	9.9
HCC38	274.5	57.8
BT549	56.7	15.8
BT20	364.6	139.9
MDA-MB-231	208.1	84.0
***BRCA1*-mutated/Acquired PARP Inhibitor Resistance**		
MDA-MB-436-RR	201.2	37.5
***BRCA1*-mutated/Primary PARP Inhibitor Resistance**		
SUM149PT	51.5	15.9
HCC1937	125.3	43.1

Supplemental Experimental Procedures

Assay for Homologous Recombination proficiency. U2OS pDR-GFP cells (provided by Maria Jasin, Memorial Sloan Kettering Cancer Center) were transfected with an I-SceI cutting enzyme in the presence of vehicle or 15 nM dinaciclib, trypsinized, washed in PBS and analyzed for GFP expression by flow cytometry (Pierce et al., 1999) using FloJo software.

CRISPR/CAS9 targeting. Lenti-CRISPR/Cas9 vectors targeting CDK12 and CDK9 were provided by Jean Zhao, Dana-Farber Cancer Institute. Viral infection was carried out as previously described (Wang et al., 2015).

Immunohistochemical Staining. Formalin-fixed, paraffin-embedded sections of harvested xenografts were stained with antibodies recognizing Ki-67 (MIB-1, Dako), geminin (Protein Tech Group, 10802-1-AP), Aurora B (Abcam ab45145) and phospho-RB [pT356] (Invitrogen 44-578). Staining was scored manually or quantified using Aperio image analysis.

Assay for Nucleotide Excision Repair (NER) proficiency. Monitoring of NER was performed as previously described (Dreze et al., 2014). Briefly, growing cells were left intact or irradiated with 15J/m^2 UV-C and returned to the incubator for 5 or 120 min. The cells were then fixed with -20C methanol for 20 minutes. After rehydration the cells were stained for (6-4)photoproducts using the DDB2 proteo-probe. The DDB2 proteo-probe fluorescent staining was imaged using a Zeiss automated microscope platform. Images were analyzed and quantified using the CellProfiler software. Graphs show the ratio of DDB2 staining measured between 5 and 120 min after subtraction of the background found in intact cells.

BH3 Profiling Assay. BH3 profiling was performed as previously described (Ni et al., 2011; Sarosiek et al., 2013). 15 μL of BH3 peptides or recombinant proteins and 5 mM succinate was deposited into each well in a 384-well plate, to which permeabilized cells were added. After agitation inside the plate reader, fluorescence at 590 nM was measured every 5 min at room temperature. Peptide treatments that were used corresponded to the BH3 domains of the BCL-2 family proteins, and their respective sequences are as follows:
BIM: MRPEIWIAQELRRIGDEFNA; BID: EDIIRNIARHLAQVGDSMDR (New England Peptide, Gardner MA). Relative mitochondrial depolarization was defined as the magnitude of mitochondrial depolarization resulting from BH3 peptide treatment as compared to DMSO and positive control FCCP (p-trifluoromethoxy carbonyl cyanide phenyl hydrazone) (Sigma-Aldrich). The percentage of mitochondrial depolarization was calculated by comparing the JC1 signal (mitochondrial polarization) in cell lines treated with each peptide or protein concentration in the following manner: % Mitochondrial Depolarization = [R(t) - F(t)] / [R(t) – FCCP(t)] * 100, where R(t) is the fluorescence value in the reference sample (DMSO), F(t) is the fluorescence value in the test sample (peptide or protein) and FCCP(t) is the fluorescence value in the positive control sample (FCCP) at a time (t) and averaged over the dynamic portion of depolarization curves.

Supplemental References

Dreze M, Calkins AS, Galicza J, Echelman DJ, Schnorenberg MR, Fell GL, et al. Monitoring repair of UV-induced 6-4-photoproducts with a purified DDB2 protein complex (2014). PLoS One *9,* e85896.

Martin, M.P., Olesen, S.H., Georg, G.I., and Schönbrunn, E. (2013). Cyclin-dependent kinase inhibitor dinaciclib interacts with the acetyl-lysine recognition site of bromodomains. ACS Chem. Biol. *8,* 2360–2365.

Mita, M.M., Mita, A.C., Moseley, J., Poon, J., Small, K.A., Jou, Y., Kirschmeier P., Zhang D., Statkevich, P., Sankhala, K.K., Sarantopoulos, J. Cleary, J.M., Chirieac, L.R., Rodig, S., Bannerji, R., Shapiro, G. (2011). A phase I study of the CDK inhibitor dinaciclib (SCH727965) administered every 3 weeks in patients with advanced malignancies: final results. J Clin Oncol *29 suppl.,* A3080 [abstract].

Ni Chonghaile T, Sarosiek KA, Vo TT, Ryan JA, Tammareddi A, Moore Vdel G, Deng J, Anderson KC, Richardson P, Tai YT, Mitsiades CS, Matulonis UA, Drapkin R, Stone R, Deangelo DJ, McConkey DJ, Sallan SE, Silverman L, Hirsch MS, Carrasco DR, Letai A. (2011). Pretreatment mitochondrial priming correlates with clinical response to cytotoxic chemotherapy. Science *334,* 1129-1133.

Pierce, A.J., Johnson, R.D., Thompson, L.H., and Jasin, M. (1999). XRCC3 promotes homology-directed repair of DNA damage in mammalian cells. Genes Dev. *13*, 2633-2638.

Sarosiek KA, Chi X, Bachman JA, Sims JJ, Montero J, Patel L, Flanagan A, Andrews DW, Sorger P, Letai A. (2013). BID preferentially activates BAK while BIM preferentially activates BAX, affecting chemotherapy response. Mol. Cell *51,* 751-765.